CrystEngComm

Cite this: *CrystEngComm*, 2012, **14**, 4396–4406

www.rsc.org/crystengcomm

PAPER

Trans-keto* form detection in non photochromic *N*-salicylidene aminomethylpyridines†‡

François Robert, Pierre-Loïc Jacquemin, Bernard Tinant and Yann Garcia*

Received 3rd January 2012, Accepted 5th April 2012
DOI: 10.1039/c2ce00006g

Five *N*-(5-chloro)salicylidene aminomethylpyridine derivatives were successfully synthesized and their structural and solid state optical properties analyzed. Yellow crystalline powders of $\mathbf{CH_2L^3}$ and $\mathbf{CH_2L^{3-4}Cl}$ present both thermo- and photochromism whereas $\mathbf{CH_2L^2}$ and $\mathbf{CH_2L^4}$ do not show any switching properties, as probed by diffuse reflectance spectroscopy. Contrary to structural–optical expectations, the non-photochromic $\mathbf{CH_2L^2}$ molecule ($P2_1/n$) shows an open crystal structure, and photochromic molecules $\mathbf{CH_2L^{3-4}Cl}$ ($P2_1/c$) present a closed crystal packing, revealed by single crystal X-ray diffraction, which is typical of exclusively thermochromic molecules. After UV irradiation, *trans*-keto* emission observation in $\mathbf{CH_2L^2}$ and $\mathbf{CH_2L^4}$ indicates the unexpected formation of the *trans*-keto form in these non-photochromic anil molecules. Radiative relaxation of the *trans*-keto* form is in addition detected, for the first time, by fluorimetry for all *N*-salicylidene molecules of the series, whatever their switchable chromic properties.

Introduction

Solid state photochromism corresponds to a reversible photo-induced equilibrium between two species presenting different absorption spectra.[1] This switching phenomenon, which is potentially encountered in inorganic/organic species, can have several origins such as a redox reaction,[2] electron–hole pair generation,[3] spin crossover,[4] photocyclization,[5] coordination change,[6] photo-isomerisation,[7] or both[8] a tautomerisation and bond cleavage,[9] which can be associated to a reversible modification of the geometric structure, dielectric constant, magnetic susceptibility,[8,10,11] and refractive index.[5] Organic photochromism, which is rarely observed in the crystalline state,[5] has been optimized for information storage,[12,13] molecular machines,[14] photo optical switches,[15] displays,[16] sensors,[17] and non-linear optics,[18] and therefore still attracts considerable attention. Among the rare classes of molecules that exhibit both thermo and photochromism in the crystalline state, *N*-salicylidene aniline can be highlighted.[19–22] Thermochromism, which corresponds to a temperature-induced reversible colour change,[23] results from a tautomeric thermal equilibrium between the uncoloured enol form and the yellow *cis*-keto form. Irradiation of the enol and *cis*-keto forms at λ = 365 nm and 436 nm, respectively, produces the red metastable *trans*-keto form thanks to a *cis*/*trans* photo-isomerisation of the C–N bond (Scheme 1).

The photochemical process associated with photochromism has been described.[24–26] UV irradiation of the enol form leads to an excited enol form (enol*) that can fluoresce or rapidly undergo a fast tautomerisation to produce the excited *cis*-keto* form. The *cis*-keto* form can also fluoresce or undergo photo-isomerisation to produce the excited *trans*-keto* form by photo-isomerisation, which is described to be non-fluorescent. Non-radiative relaxations enol* → enol and *cis*-keto* → *cis*-keto and radiative relaxation *trans*-keto* → *trans*-keto have been considered up to now as negligible.[24–26] Back reaction from *trans*-keto to *cis*-keto and enol forms is either thermally or photochemically induced.

N-salicylidene aniline derivatives have been distinguished, on a first approximation, by comparing their crystal structure and optical properties at room temperature.[27] Thermochromic molecules present a planar conformation, with a low dihedral

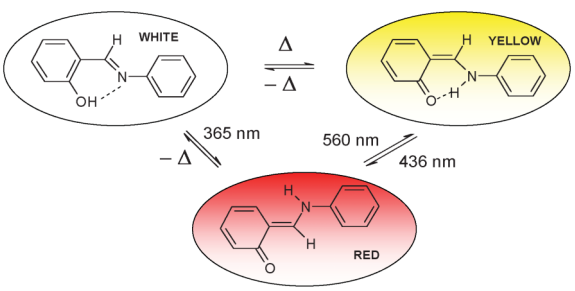

Scheme 1 Thermochromism and photochromism pathways of *N*-salicylidene aniline.

Institute of Condensed Matter and Nanosciences, MOST – Inorganic Chemistry, Université Catholique de Louvain, Place L. Pasteur 1, 1348, Louvain-la-Neuve, Belgium. E-mail: yann.garcia@uclouvain.be; Fax: +32(0) 1047 2330; Tel: +32(0) 1047 2831

† This work is dedicated to the memory of our colleague, Prof. Jean-Louis Habib Jiwan.

‡ Electronic supplementary information (ESI) available: X-ray powder diffractograms of $\mathbf{CH_2L^3Cl}$ and $\mathbf{CH_2L^4Cl}$. CCDC reference numbers 854915 ($\mathbf{CH_2L^2}$) and 854916 ($\mathbf{CH_3L^3Cl}$). For ESI and crystallographic data in CIF or other electronic format see DOI: 10.1039/c2ce00006g

angle between aromatic planes below 25°, and are closely packed in their crystal lattice. Such structures are stabilized by π–π and/or CH–π interactions.[28] In contrast, photochromic molecules are defined by their non-planar character, with a dihedral angle greater than 25°, and an open crystal packing which is favourable for a conformation change, allowing the stabilization of the *trans*-keto form.[29] Nevertheless, *N*-salicylidene aminopyridine derivatives have revealed intriguing features.[30] *N*-salicylidene-3-aminopyridine (**L^3**) first displays a close packing and a planar geometry, but presents both thermochromism and photochromism at room temperature. Secondly, *N*-salicylidene-4-aminopyridine (**L^4**), which is highly twisted and packed in an open structure, is exclusively thermochromic.[30] Theoretical studies of those model systems allowed to discuss the photoisomerization mechanism inside the crystal lattice and to compute energies for *cis* and *trans*-keto forms in both ground state and excited states, allowing to predict the best conditions for photochromism observation when the activation barrier between *cis*-keto* and *trans*-keto* forms is low.[28,30]

In this work, we have studied the influence of the increase of flexibility and electronic conjugation loss among *N*-salicylidene aminopyridine derivatives on the optical properties after the introduction of a methylene spacer between salicyl and pyridine rings (Scheme 2), as first postulated by Hadjoudis *et al.* for *N*-salicylidenebenzylamines.[27] More precisely, *N*-salicylidene-2-aminomethylpyridine (**CH$_2$L^2**), *N*-salicylidene-3-aminomethylpyridine (**CH$_2$L^3**), *N*-salicylidene-4-aminomethylpyridine (**CH$_2$L^4**), 5-chlorosalicylidene-3-aminomethylpyridine (**CH$_2$L^{3}Cl**) and 5-chlorosalicylidene-4-aminomethylpyridine (**CH$_2$L^{4}Cl**) were prepared, characterized and investigated by using complementary methods such as X-ray diffraction, UV-visible diffuse reflectance spectroscopy and fluorimetry. Increasing flexibility of these molecules allows the unexpected fluorescence of the *trans*-keto form of a functional Schiff base derived from aniline, to be detected, for the first time, at room temperature.

Results and discussion

Syntheses and crystallization

The synthesis of *N*-salicylidene aminomethylpyridine derivatives was initially carried out following reported procedures (e. g. reflux in ethanol followed by recrystallization[31–33] and solvent free synthesis[34]). The products appeared however to be sensitive to residual water (provoking hydrolysis leading to salicylaldehyde impurities) or high temperature (leading to a very fast degradation) and a modified synthetic procedure had then to be developed. A Dean–Stark set-up was used with benzene (instead of toluene in order to reduce the reflux temperature) and the resulting crude yellow oil was purified by several sonication cycles in hexane. Target molecules were obtained in large amounts with excellent purity as yellow microcrystalline powders, except for **CH$_2$L^4**, which was amorphous as concluded from powder X-ray diffraction (PXRD). 5-Chlorosalicylidene-2-aminomethylpyridine (**CH$_2$L^{2}Cl**) was prepared similarly but could not be isolated as a pure compound.

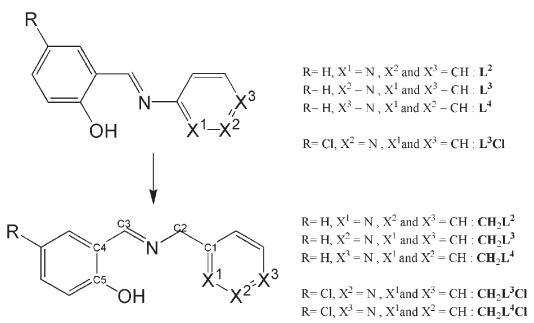

Scheme 2 Molecular schemes of *N*-salicylidene aminopyridines and *N*-salicylidene aminomethylpyridines where a methylene spacer is introduced between the two aromatic rings.

Single crystals were obtained after one week, as yellow blocks (for **CH$_2$L^2**, **CH$_2$L^3**) and yellow plates (for **CH$_2$L^{3}Cl**), by recrystallization from a hot hexane mother solution followed by slow evaporation, and analyzed by X-ray diffraction (see next section).

Structural aspects

Crystal structure of *N*-salicylidene 2-amino-methylpyridine (CH$_2$L^2). The **CH$_2$L^2** molecule crystallizes in the monoclinic space group $P2_1/n$ at 125(2) K (Table 1). The bond lengths C2–O16 (1.352(2) Å) and C1–C7 (1.458(2) Å) indicate single bonds whereas the bond length C7–N8 of 1.278(2) Å (Table 2) is typical of a double bond which identifies the enol form (Fig. 1a). The dihedral angle between the two aromatic rings (Φ = 81(1)°) is much higher than the usual range of angles observed in *N*-salicylidene aniline aminopyridine derivatives (5–49°).[30] It could take its origin from the increase in molecular flexibility induced by the methylene spacer between aromatic rings, which implies a large torsion angle Γ of 114(1)° (Table 2). An intramolecular hydrogen bond is observed between imine and alcohol functions (O16–H16···N8) with a distance of 1.74(3) Å (Table 3). Two intermolecular C–H···π interactions are also

Table 1 Crystal data and structure refinement for **CH$_2$L^2**, **CH$_2$L^3** and **CH$_2$L^{3}Cl**

	CH$_2$L^2	**CH$_2$L^3** [31]	**CH$_2$L^{3}Cl**
Empirical formula	$C_{13}H_{12}N_2O$	$C_{13}H_{12}N_2O$	$C_{13}H_{11}N_2OCl$
M_r	212.25	212.25	246.69
T/K	125(2)	297(1)	120(2)
Crystal system	Monoclinic	Monoclinic	Monoclinic
Space group	$P2_1/n$	$P2_1/n$	$P2_1/c$
a/Å	9.863(3)	10.49(1)	13.864(4)
b/Å	10.363(3)	9.002(4)	6.004(2)
c/Å	11.563(3)	12.42(1)	14.041(4)
β (°)	113.28(2)	109.10(4)	103.95(2)
V/Å^3	1085.6(5)	1109(2)	1134.3(6)
Z	4	4	4
ρ_{calcd}/Mg m^{-3})	1.299	1.271	1.445
F(000)	448	448	512
μ/mm^{-1}	0.084	0.08	0.32
Crystal size/mm	0.4 × 0.3 × 0.3	0.1 × 0.3 × 0.4	0.5 × 0.4 × 0.1
θ_{max} (°)	26.37	25.00	26.39
Reflections collected/unique	8564/2120	2411/886	19 898/2257
R_{int}	0.045	0.053	0.053
R_1 [$I > 2\sigma(I)$]	0.0475 [1931]	0.049 [156]	0.0409 [2167]
wR_2	0.123	—	0.113
Largest diff. peak/hole	0.353 and −0.214	—	0.251 and −0.287

Table 2 Selected bond lengths and angles for CH_2L^2, CH_2L^3 and CH_2L^3Cl

	CH_2L^2	CH_2L^3 [31]	CH_2L^3Cl
Φ (°)	81(1)	90(1)	72(1)
Γ (°)	114(1)	112(1)	117(1)
Dist. (Å)[a]	5.99	5.51	5.54
C2–C1 (Å)[b]	1.509(2)	1.507(7)	1.512(2)
N–C2 (Å)[b]	1.459(2)	1.459(5)	1.469(2)
C3–N (Å)[b]	1.278(2)	1.269(5)	1.279(2)
C4–C3 (Å)[b]	1.458(2)	1.450(7)	1.463(2)
C5–C4 (Å)[b]	1.410(3)	1.403(6)	1.406(2)
C5–O (Å)[b]	1.352(2)	1.348(5)	1.354(2)

[a] Average distance between molecule centroids. [b] Distances with respect to Scheme 2.

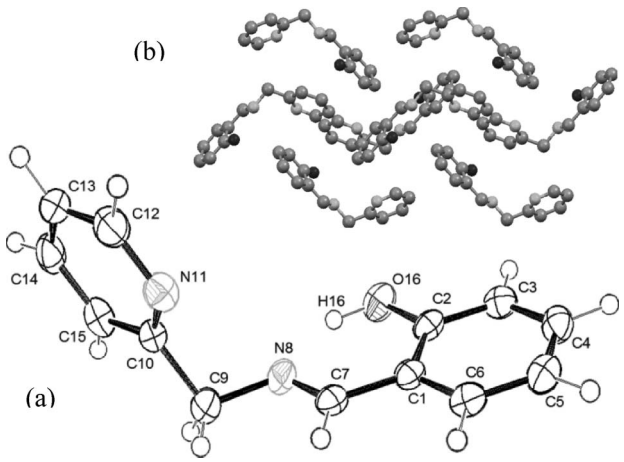

Fig. 1 (a) ORTEP view of the asymmetric part of the unit cell of CH_2L^2, showing 50% probability displacement ellipsoids. (b) View of the crystal packing of CH_2L^2 along the *c* axis. H atoms were omitted for clarity.

present between H14 and centroids of salicyl ring (C1–C2–C3–C4–C5–C6, d = 2.88 Å), and between H7 and pyridine (N11–C10–C11–C12–C13–C14–C15, d = 2.65 Å) (Table 4). The large intermolecular distance between molecules (~6 Å, Table 2) qualifies the crystal packing as an open structure (Fig. 1b), which is typical of photochromic molecules.[27]

Crystal structure of 5-chloro-*N*-salicylidene 3-aminomethylpyridine (CH_2L^3Cl). The crystal structure of CH_2L^3Cl was solved at 120(2) K. The Schiff base crystallizes in the monoclinic space group *P*21/c (Table 1) and the enol form is observed in the asymmetric unit as deduced from bond lengths N8–C7 (1.279(2) Å) and C2–O16 (1.354(2) Å) (Table 2). As observed for CH_2L^2, the molecule flexibility is responsible for the large distortion angle (Φ = 72(1)°) (Table 2 and Fig. 2a). CH_2L^3Cl presents an intramolecular hydrogen bond (O16–H16···N8) with a distance of 1.81(3) Å (Table 3) that can be considered similar to the hydrogen bond observed in CH_2L^2 and CH_2L^3.[31] Several intermolecular interactions contribute to the generation of a dense supramolecular network (Fig. 2b). One intermolecular hydrogen bond between C13H13 and N112 of two pyridine rings thus forming supramolecular dimers (Table 3), two C–H···π interactions between C7–H7 and the benzene ring and between C15–H15 and the pyridine group, and one π–π stacking (3.826(6) Å) between two benzene moieties (Table 4) lead to a closed structure, typical of thermochromic molecules.[27]

Single crystals of CH_2L^3 were identical to the known polymorph, which shows an open structure with an intermolecular distance between centroids of 5.5 Å, as confirmed by X-ray diffraction.[31] Isostructurality of CH_2L^4Cl with CH_2L^3Cl was established by powder X-ray diffraction (Fig. S1, ESI‡).

Optical properties

Diffuse reflectance spectroscopy. Yellow crystalline powders of CH_2L^3, CH_2L^3Cl and CH_2L^4Cl turn white on cooling to 77 K (Fig. 3). On warming back to 298 K, their yellow colour is recovered. This reversible colour change is due to a thermal tautomerisation from a yellow *cis*-keto form (at 298 K) towards a white enol form at lower temperature.[23] Irradiation under visible light (λ = 450 nm) for 10 min leads to an orange coloration for these three molecules, which is best marked for CH_2L^3Cl (Fig. 4). CH_2L^2 and CH_2L^4 however do not present any thermo/photochromic properties.

Diffuse reflectance spectra were recorded on pure powder samples and a Kubelka–Munk (KM) treatment was applied (Fig. 3). It was not relevant dilute these samples, as is routinely done for other compounds, because matrix effects can dramatically modify the keto–enol equilibrium that is effective for *N*-salicylidene aniline molecules,[9,35–38] thus preventing any reliable comparative study. In each spectrum, a large intense band, attributed to the enol form, is observed in the UV range. A bathochromic shift (of about 35 nm) of the right limit of this band is noted between CH_2L^2, CH_2L^4Cl and CH_2L^3Cl.

Another band, corresponding to the *cis*-keto form, is located in the visible region. Although this signal is observed in all spectra, its relative intensity is different, increasing from (CH_2L^2, CH_2L^4Cl and CH_2L^4) < CH_2L^3Cl < CH_2L^3. For $CH_2L^{3-4}Cl$ two contributions are noted for the *cis*-keto band (with maxima at 420 and 460 nm) which are attributed to two different conformations of the *cis*-keto form (Fig. 3).

Irradiation at 450 nm of CH_2L^3, CH_2L^3Cl and CH_2L^4Cl leads to a new band around 500 nm attributed to the population of the metastable *trans*-keto form resulting from photo-isomerisation (Fig. 4).

Table 3 Intra- and inter-molecular hydrogen bonds in CH_2L^2, CH_2L^3 and CH_2L^3Cl

Molecule	D–H···A	D–H (Å)	H···A (Å)	D···A (Å)	D–H···A (°)	Ref.
CH_2L^2	O16H16···N8	0.96(3)	1.74(3)	2.602(2)	149(2)	This work
CH_2L^3	O16H16···N8	1.02(5)	1.73(5)	2.571(5)	137(4)	31
CH_2L^3Cl	O16H16···N8	0.87(2)	1.81(3)	2.616(2)	153(2)	This work
	C13H13···N112[a]	0.98(2)	2.56(2)	3.459(2)	152(2)	

[a] N112 is generated by the symmetry operation 3 − *x*, 1 − *y*, −*z*.

Table 4 Inter-molecular π–π stacking and C–H···π interactions in CH_2L^2, CH_2L^3 and CH_2L^3Cl

	Atoms involved 1	Atoms involved 2	d (Å)[a]	Angle (°)[b]
CH_2L^2	N11–C10–C15–C14–C13–C12	C7–H7	2.65(2)	2(1)
	C1–C2–C3–C4–C5–C6	C14–H14	2.88(2)	8(1)
CH_2L^3 [31]	C1–C2–C3–C4–C5–C6	C11–H8	2.85(1)	3(1)
CH_2L^3Cl	C1–C2–C3–C4–C5–C6	C1–C2–C3–C4–C5–C6	3.83(1)	0(1)
	C1–C2–C3–C4–C5–C6	C7–H7	2.81(2)	5(1)
	N12–C11–C10–C15–C14–C13	C15–H15	2.78(1)	6(1)
	C1–C2–C3–C4–C5–C6	C1–C2–C3–C4–C5–C6	3.826(2)	0(1)

[a] π–π stacking: distances between ring centroids; C–H···π: distances between H atoms and ring centroids. [b] π–π stacking: angles between ring planes; C–H···π: angles between C–H axis and ring planes.

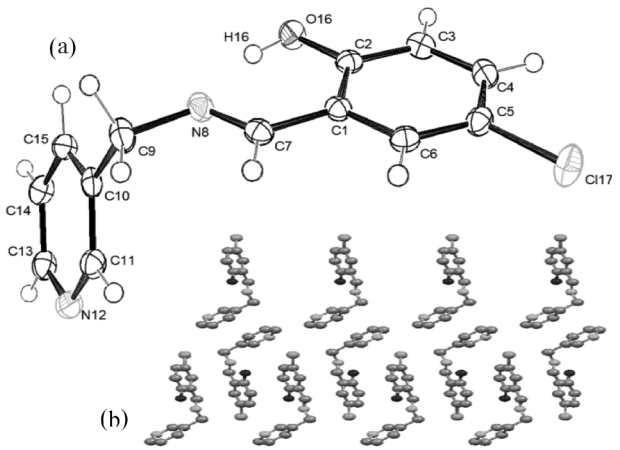

Fig. 2 (a) ORTEP view of the asymmetric part of the unit cell of CH_2L^3Cl, showing 50% probability displacement ellipsoids. (b) View of the crystal packing of CH_2L^3Cl along the *b* axis. H atoms were omitted for clarity.

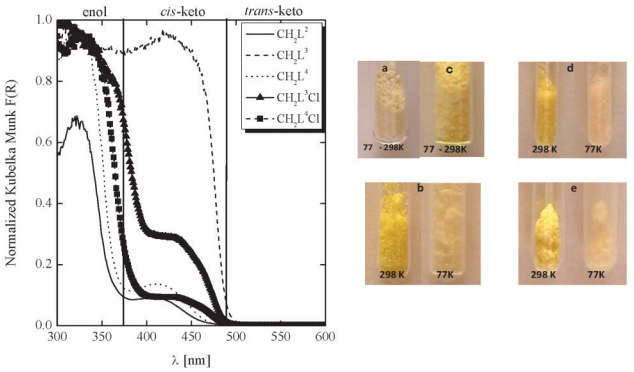

Fig. 3 Left: Kubelka–Munk spectra of CH_2L^{2-4} and $CH_2L^{3-4}Cl$ at 298 K. Right: Photographs of powders of CH_2L^2 (a) and CH_2L^4 (c) over the temperature range 298–77 K and of CH_2L^3 (b), CH_2L^3Cl (d) and CH_2L^4Cl (e) at 298 and 77 K. Thermochromism is clearly identified for b, d and e.

For CH_2L^3, the band maximum is slightly shifted to 520 nm. Photo-isomerisation is also efficient at 365 nm as shown in Fig. 4a. For CH_2L^3Cl, two unresolved bands with maxima at 510 and 540 nm are detected (Fig. 4b). Their contribution may be related to the formation of two different conformations of the *trans*-keto form which could arise from the large flexibility given

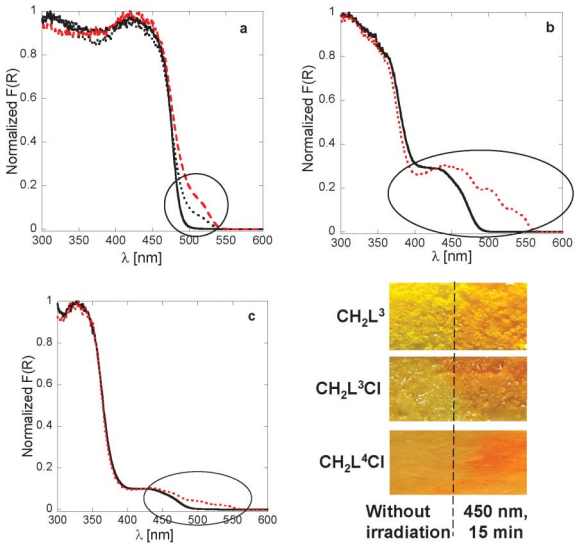

Fig. 4 Kubelka–Munk spectra at 298 K of (a) CH_2L^3 before (black line) and after irradiation at 365 nm (black dotted line) and at 450 nm (red dotted line), for 15 min and 5 min, respectively; (b) CH_2L^3Cl before (black line) and after irradiation at 450 nm for 5 min (red dotted line); (c) CH_2L^4Cl before (black line) and after irradiation at 450 nm for 10 min (red dotted line). The circles highlight the increase of the intensity of the *trans*-keto band.

by the methylene spacer. The Kubelka–Munk spectrum of CH_2L^4Cl reveal the same profile as for CH_2L^3Cl, with two weak bands located at 505 and 530 nm, arising from the *trans*-keto form (Fig. 4c).

The reversibility of the *cis*/*trans* isomerisation was investigated by time dependent diffuse reflectance spectroscopy. Irradiation of CH_2L^3Cl at 450 nm for 20 min leads to a large increase of the intensity of the signal of the *trans*-keto form (at 546 nm). Thermal relaxation to the *cis*-keto form is complete after 3600 s, as shown in Fig. 5a. The relaxation appears to be elaborated and contains more than one chemical relaxation pathway. Attempts to fit this curve with a single exponential function failed. Reverse photo-switching of the *trans*-keto → *cis*-keto form can be achieved by irradiating the *trans*-keto band at 546 nm, thus demonstrating the reproducibility of the switch. The cycles were repeated several times without significant alteration as shown in Fig. 5b for two cycles. The thermal and photochemical relaxation of the *trans*-keto form of CH_2L^3 and CH_2L^4Cl could not be analyzed because of a too fast thermal relaxation.

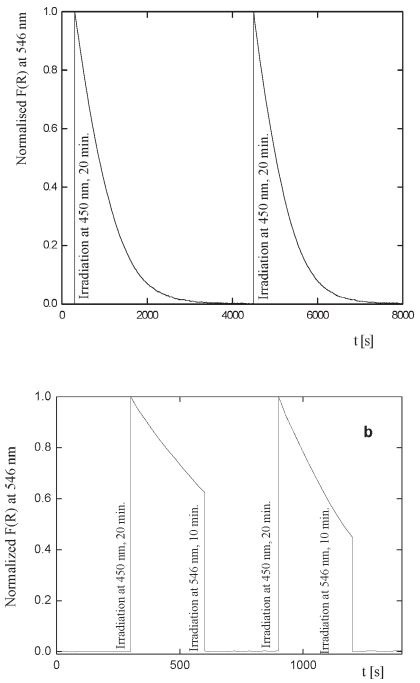

Fig. 5 Time dependence of the Kubelka–Munk function (F) of $\mathbf{CH_2L^3Cl}$ at 546 nm showing: (a) a fast thermal relaxation of the metastable *trans*-keto form after irradiation; (b) reversibility of the *cis*/*trans* isomerisation with irradiation cycles at 450 and 546 nm, respectively.

Solid state fluorimetry. All molecules were analyzed by solid state fluorimetry at room temperature in order to study photochemical processes involved in photochromism observation. The results are presented in two different groups based on the presence of photochromism ($\mathbf{CH_2L^3}$, $\mathbf{CH_2L^3Cl}$, $\mathbf{CH_2L^4Cl}$)) (Fig. 6 and 7) or its absence ($\mathbf{CH_2L^2}$ and $\mathbf{CH_2L^4}$) (Fig. 8).

In emission measurements, the excitation wavelength is locked on a selected area of the diffuse reflectance spectrum corresponding to the band maximum of the prototropic form of the *N*-salicylidene aminomethylpyridine molecule to be analyzed,

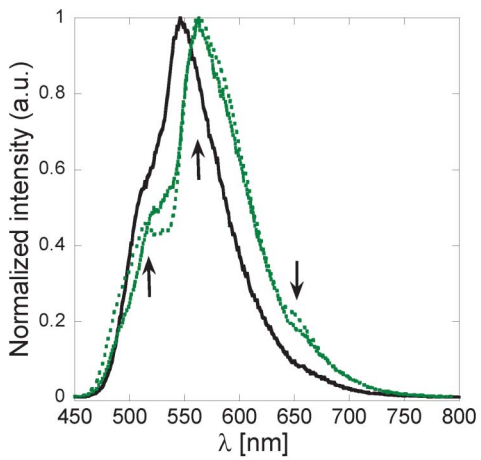

Fig. 6 Emission spectra of solid samples of $\mathbf{CH_2L^3}$ (bold black line), and $\mathbf{CH_2L^3Cl}$ (dotted green line) and $\mathbf{CH_2L^4Cl}$ (bold green line) at 298 K (λ_{exc} = 430 nm). The arrows indicate the three emission contributions discussed in the text for $\mathbf{CH_2L^{3-4}Cl}$.

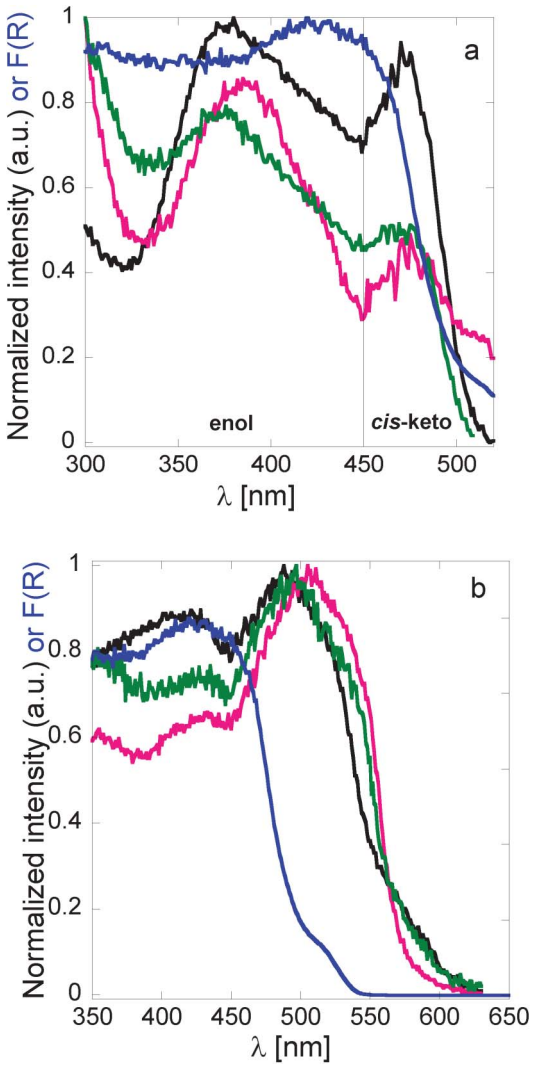

Fig. 7 Excitation spectra of solid samples of $\mathbf{CH_2L^3}$ (black line) and $\mathbf{CH_2L^3Cl}$ (green line) and $\mathbf{CH_2L^4Cl}$ (pink line) at 298 K at: (a) λ_{em} = 540 nm; (b) λ_{em} = 650 nm. The blue curve represents the diffuse reflectance spectrum of $\mathbf{CH_2L^3}$ after irradiation at 450 nm during 5 min. The enol, *cis*- and *trans*-keto ranges are observed from UV to ~400 nm, from 400 to 500 nm and between 500 and 550 nm, respectively.

and the emission wavelength is scanned. The spectrum contains all emissions driven from the generated excited form (*e.g.* irradiating $\mathbf{CH_2L^3}$ at 370 nm leads to the enol* form and emissions of enol* → enol (A) and *cis*-keto* → *cis*-keto (B), as depicted on Scheme 3). In the excitation mode, the emission wavelength is fixed at its maximum and an excitation spectrum is scanned. For example, we shall focus hereafter on the *cis*-keto*→ *cis*-keto emission at 540 nm and scan excitation wavelengths. Excitation spectrum is expected to reveal two bands corresponding to pathways C (enol→enol*→*cis*-keto*) and D (*cis*-keto→*cis*-keto*) leading to the formation of the monitored emitting excited state (Scheme 3).

Solid state emission spectra of $\mathbf{CH_2L^3}$ and $\mathbf{CH_2L^{3-4}Cl}$ were thus recorded at λ_{exc} = 370 nm and 430 nm which corresponds to the absorption bands of enol and *cis*-keto forms, respectively (Fig. 3), and at λ_{exc} = 520 nm corresponding to the *trans*-keto form, obtained after irradiation (Fig. 4).

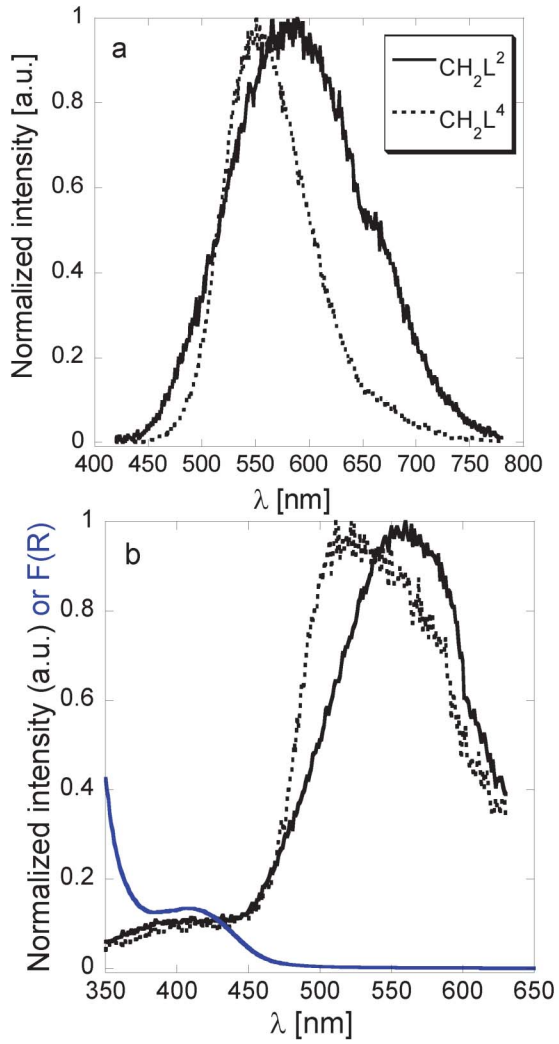

Fig. 8 (a) Emission spectra of solid samples of $\mathbf{CH_2L^2}$ and $\mathbf{CH_2L^4}$ at 298 K (λ_{exc} = 400 nm). (b) Excitation spectra of $\mathbf{CH_2L^2}$ (bold line) and $\mathbf{CH_2L^4}$ (dotted line) at 298 K (λ_{em} = 655 nm and 660 nm, respectively). The blue curve represents the diffuse reflectance spectrum of $\mathbf{CH_2L^2}$. The *cis*- and *trans*-keto ranges are observed from 400 to 450 nm and between 450 and 650 nm, respectively.

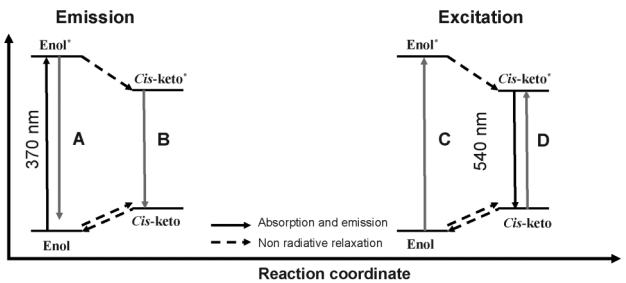

Scheme 3 Photochemical processes evidencing two radiative relaxation pathways in emission mode (A, B) and two absorption pathways in excitation mode (C, D) for *N*-salicylidene aniline derivatives.

These emission spectra were also recorded on pure samples in order to avoid matrix effect which can strongly modify the population of keto/enol forms.[9,35–38] In the following, we shall only discuss emission spectra related to λ_{exc} = 430 nm because of its high resolution (Fig. 6). Three bands are detected with emission maxima at approximately 520, 540 and 610 nm for $\mathbf{CH_2L^3}$, and 530, 570 and 660 nm for $\mathbf{CH_2L^{3-4}Cl}$, whose origin shall be addressed below.

Excitation spectra of $\mathbf{CH_2L^3}$ and $\mathbf{CH_2L^{3-4}Cl}$ at λ_{em} = 540 nm (or 520 nm) indicate two contributions (Fig. 7a). A very high intensity is detected from UV to ~450 nm which can be attributed to the enol form absorption (Pathway C in Scheme 3). This signal presents several unresolved contributions which are probably due to different electronic transitions present in this form.[39] Another excitation band is observed between 450 and 500 nm, which is attributed to the *cis*-keto form, by comparison with diffuse reflectance spectroscopy (Pathway D in Scheme 3).[39] Thus, the emission bands centred at 520 and 540 nm in Fig. 6 originate from the radiative de-excitation of the *cis*-keto* form (pathway B in Scheme 3), which is produced from the absorption of the enol form (which undergoes then an excited state fast tautomerisation from the enol* form) and from the *cis*-keto form in the ground state.

Excitation spectra recorded at λ_{em} = 650 nm (Fig. 7b) reveal the same two contributions with a third intense band centred at λ_{max} ~500 nm, which can be clearly assigned to the absorption of the *trans*-keto form by comparison with diffuse reflectance spectrum also recalled on Fig. 7b. The emission at 610 and 660 nm (Fig. 6) can thus be assigned to the radiative relaxation of the *trans*-keto* form, which can be formed through the absorption of enol, *cis*-keto and *trans*-keto forms in their ground state. It is worthwhile to note that the emission of the *trans*-keto form of a functional Schiff base derived from aniline is observed for the first time.

Similar solid state fluorimetry experiments were carried out on non-photochromic molecules ($\mathbf{CH_2L^2}$ and $\mathbf{CH_2L^4}$). At λ_{exc} = 400 nm, which corresponds to the *cis*-keto form absorption (Fig. 3), both emission spectra are very similar and present a broad band (Fig. 8a) which is composed of two contributions at ~580 and 660 nm for $\mathbf{CH_2L^2}$, and ~550 and 650 nm for $\mathbf{CH_2L^4}$. The origin of these contributions could be elucidated by excitation spectra recorded at λ_{em} = 655 and 660 nm for $\mathbf{CH_2L^2}$ and $\mathbf{CH_2L^4}$, respectively (Fig. 8b). Interestingly, although the most intense emission peak (around 600 nm) comes from the radiative relaxation of the *cis*-keto* form, as observed for photochromic molecules described above, the excitation spectra at 655–660 nm show high intensity in the whole visible range studied.

Indeed, in addition to a signal between 350 nm and 450 nm coming from enol and *cis*-keto absorptions, an intense band is noted between 450 and 650 nm, centred at 560 and 530 nm for $\mathbf{CH_2L^2}$ and $\mathbf{CH_2L^4}$, respectively. As this additional band corresponds to the *trans*-keto form absorption, we can conclude that the shoulder observed at lowest energy in the emission spectra of $\mathbf{CH_2L^2}$ and $\mathbf{CH_2L^4}$ (Fig. 8a) originates from the radiative de-excitation of the *trans*-keto* form coming from the absorption of the enol, *cis*-keto and *trans*-keto forms, as previously pointed out for photochromic molecules $\mathbf{CH_2L^3}$ and $\mathbf{CH_2L^{3-4}Cl}$.

Discussion

Five *N*-salicylidene aminomethylpyridine derivatives were successfully synthesized and their structural and solid state optical

properties analyzed. Three molecules, CH_2L^3 and $CH_2L^{3-4}Cl$, present both thermo- and photochromism in contrast to CH_2L^2 and CH_2L^4, which are not switchable. Surprisingly, the absence of chromic properties for CH_2L^2 contradicts a previous claim,[40] as its crystal packing shows molecules packed with long intermolecular distances, and nevertheless the molecule is not photochromic.

Solid state fluorimetry was thought in order to probe radiative relaxations and afford a better understanding of the energy scheme involved during thermo- and photochromic processes. This approach is rather unusual taking into account that the literature is relatively silent in systematic fluorescence studies for this class of molecules. It was claimed for instance that *N*-salicylidene aniline derivatives showed exclusively one emission band attributed to the de-excitation of the *cis*-keto* form.[29,41,42] In this work, we have successfully completed the emission scheme by finding two other emissions coming from the enol* and *trans*-keto* forms, for the first time. Solid state fluorimetry thus provides new insights into the formation and switchable properties of the *trans*-keto form, which was systematically associated, on a first basis, to its observation by diffuse reflectance spectroscopy.

Indeed, all *N*-salicylidene aminomethylpyridines present a low energy emission which can be attributed to the radiative de-excitation of the *trans*-keto* form whatever, whether the molecules are originally photochromic or not. The non-detection of the *trans*-keto* form emission in earlier studies could be either due to: (i) the low resolution power of solid state fluorimetry preventing distinguishing between *cis*-keto* and *trans*-keto* emission bands or (ii) the absence of radiative relaxation of the *trans*-keto* form. Surprisingly, *trans*-keto form emission is more intense for non-photochromic molecules CH_2L^2 and CH_2L^4, suggesting that formation of *trans*-keto* form from the *cis*-keto* one is highly favourable. Therefore the *trans*-keto form is produced by light irradiation in both photochromic and non-photochromic molecules but is too unstable to be accumulated, and therefore to be detected by diffuse reflectance spectroscopy only. Indeed, even in photochromic molecules, the *trans*-keto photoproduct appears less stabilized as demonstrated by the very fast thermal relaxation of CH_2L^3 and $CH_2L^{3-4}Cl$.

The absence of photochromism in this class of molecules can be explained by considering the activation barriers heights for the keto form being either too large between *cis*-keto* and *trans*-keto* forms (barrier 1) or too low between *cis*-keto and *trans*-keto forms (barrier 2) as shown in Scheme 4. It suggests that although the *trans*-keto form is revealed in excitation spectra (Fig. 8b), it could be present as traces in non-photochromic molecules (being stabilized by crystal defects), their formation mechanism yet to be established. In this respect, a theoretical study of the distribution of these species into the crystal could be useful.[26,28]

The impact of the methyl spacer on photochromism, which was considered too in this work,[27] is difficult to predict because in addition to the loss of electronic conjugation, the CH_2 group provides more flexibility to the molecules, which leads to new molecular conformations, supramolecular interaction networks and crystal packing, as described in the crystal structures section. This study is particularly relevant taking into account that the role of flexibility on this class of molecules was only briefly

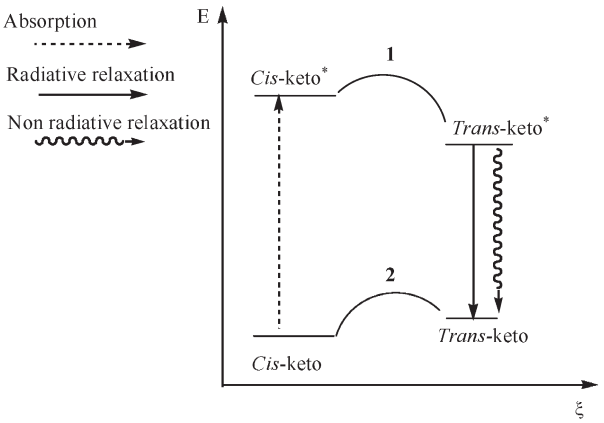

Scheme 4 Photochemical process leading to the formation of the *trans*-keto form from the *cis*-keto absorption, and to the accumulation of this form leading to photochromism observation. The activation barriers 1 and 2 are highlighted in the formation and relaxation chemical pathways of the *trans*-keto form.

considered.[43] The presence of the methylene group also induces a large change in the energy of electronic levels which leads to a modification of the shape of diffuse reflectance spectra (shifts of the bands, modification of the enol/*cis*-keto population ratio, *etc*). Moreover, the consequence of the addition of an electronic substituent onto the phenol group on the optical properties was also studied. Introduction of a chloride in *N*-salicylidene aminopyridine derivatives leads to a bathochromic shift (as observed from L^3 to L^3Cl, Fig. 9a) whereas no major effect is observed from CH_2L^3 to CH_2L^3Cl (Fig. 9b). A change in the enol/*cis*-keto signals ratio by adding the chloride substituent and the methyl group is also noted. (Fig. 9b). It could be explained considering electronic conjugation in the molecule. The proton transfer from enol to *cis*-keto form induces formation of an amine (an electron donor group) which is stabilized by the acceptor effect of the ketone and, for fully conjugated molecules like L^3 and L^3Cl, by the acceptor effect of the pyridine ring. Introducing a chloride induces competition between the mesomeric donor effect of the chloride and amines moieties, which leads to a destabilization of the *cis*-keto form. The *cis*-keto destabilization is much more important in derivatives incorporating a methyl spacer (from CH_2L^3 to CH_2L^3Cl) than in aminopyridine derivatives (from L^3 to L^3Cl) which are completely conjugated. The loss of stabilization can be also observed by solid state fluorimetry where important shifts of emission and excitation bands occur when aminomethylpyridines derivatives are compared to aminopyridine molecules.[30]

Conclusions

Increasing the flexibility of *N*-salicylidene aminopyridine derivatives allow to gain further insights into the understanding and predictions of the solid state optical properties of *N*-salicylidene derivatives, after our discussion[30] about the discrepancy of structure–optical-properties relationship, previously widely quoted in the literature,[1,29,44] and which is no longer self sufficient to predict solid state photochromism. In addition, the study of *N*-salicylidene aminomethylpyridines by fluorescence spectroscopy improves the understanding of photochemical

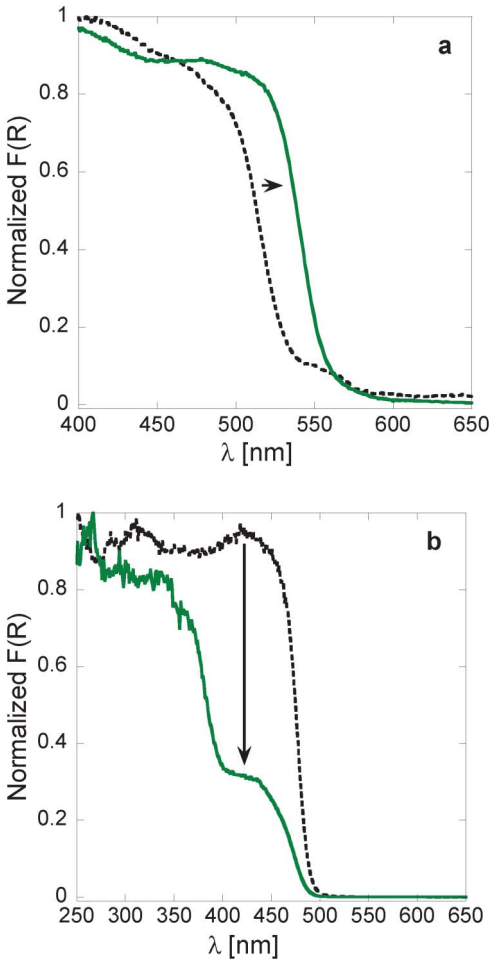

Fig. 9 Effect of the chloride substitution on the diffuse reflectance spectra of: (a) $\mathbf{L^3}$ (dotted line) and $\mathbf{L^3Cl}$ (bold line). (b) $\mathbf{CH_2L^3}$ (dotted line) and $\mathbf{CH_2L^3Cl}$ (bold line). The arrows indicate the bathochromic shift and the modification of the enol/*cis*-keto signals ratio induced by the adding of the chloride substituent.

processes involved in photochromism, by considering energies of the different excited forms and activation barriers for a better prediction.

The radiative relaxation of the *trans*-keto* form has been, for the first time, detected by fluorimetry in photochromic and, surprisingly, in non-photochromic molecules as well. The *trans*-keto form is thus obtained in both systems but a sufficient activation barrier between *trans*- and *cis*-keto forms allows the stabilization of the *trans*-keto form in its ground state. Increasing the flexibility in the different molecules seems to favour photochromism but the loss of conjugation destabilizes the keto forms. The absence of photochromism in diffuse reflectance spectroscopy after light irradiation thus does not imply the impossibility of *trans*-keto formation. The ongoing crystal engineering efforts on this class of molecules combined to the energy optimization of different forms in their excited and ground states may help towards a better optical properties control in view of potential applications (*e.g.* for sensors or displays[13]). In addition, *N*-salicylidene aminomethylpyridine derivatives can be inserted into inorganic complexes,[45] thus offering promising prospects for this class of solid state switchable organic molecules, which have recently shown useful for proper insertion, for instance, in multifunctional spin transition materials.[46,47]

Experimental

General procedures

Sonication was performed with a Branson 3510 ultrasonic bath. ^{1}H and ^{13}C NMR spectra were recorded with a Bruker AC 300 MHz instrument with the DMSO proton peak as internal standard. Mass spectroscopy data were obtained with a Thermofinnigan LCQ ion trap spectrometer by using an ESI ionization mode. HRMS were carried out on a Micromass Q-TOF 2 spectrometer using ESI mode, detecting positive ions. Infrared spectra were recorded with a Shimadzu FTIR-8400S spectrometer with KBr disks. Elementary analyses were performed at University College London. The TGA/DTA instrument used was a TA instrument SDT2960 Simultaneous. X-ray powder diffractograms were performed with a Siemens D5000 X-ray diffractometer, with a Cu anticathode ($\lambda K\alpha$ = 1.5418 Å) in Bragg–Brentano geometry (θ/θ mode). Samples were deposited on silicon after calibration with a quartz standard. Diffuse reflectance spectra were obtained with a Varian Cary 5E spectrometer by using PTFE as a reference. Spectra were measured on pure solids to avoid matrix effects. Eventual distortions in the Kubelka–Munk spectra that could result from the study of pure compounds have not been considered because no comparison with absorption spectra was necessary. The reversibility of the *cis–trans* isomerization was checked with a LOT-ORIEL 200 W high-pressure mercury Arc lamp (LSN261). *In situ* irradiations were carried out for 10 min with appropriate filters (365, 450 and 546 nm). Data that were accumulated each 30 s were normalized. Solid-state emission spectra were obtained with a Fluorolog-3 (Jobin–Yvon-Spex Company) spectrometer. Kubelka–Munk and emissions spectra were normalized to allow meaningful comparisons.

Starting materials

Solvents (benzene for gas chromatography from Fluka, hexane for analysis from Sigma-Aldrich, [d^6]-DMSO from Aldrich) and reagents (2-, 3- and 4-aminomethylpridine from Sigma-Aldrich; salicyladehyde and 5-chlorosalicyladehyde from Acros Organics) were obtained commercially and used as received.

Syntheses

N-salicylidene-2-aminomethylpyridine ($\mathbf{CH_2L^2}$), *N*-salicylidene-3-aminomethylpyridine ($\mathbf{CH_2L^3}$), *N*-salicylidene-4-aminomethylpyridine ($\mathbf{CH_2L^4}$), 5-chlorosalicylidene-3-aminomethylpyridine ($\mathbf{CH_2L^3Cl}$) and 5-chlorosalicylidene-4-aminomethylpyridine ($\mathbf{CH_2L^4Cl}$) were prepared in benzene using a Dean–Stark setup.

N-Salicylidene 2-aminomethylpyridine ($\mathbf{CH_2L^2}$): 2-Aminomethylpyridine (0.61 mL, 1 equiv., 5.88 mmol) was dissolved in benzene (25 mL) in a 100 mL round-bottom flask with a Dean–Stark setup. Salicylaldehyde (0.62 mL, 1 equiv., 5.88 mmol) was added to the solution. The coloration immediately turned to light yellow. After refluxing for 24 h, the dark yellow solution was concentrated to obtain an orange oil. The crude product was triturated in hexane affording a pure light yellow microcrystalline

solid which was filtered (0.40 g, 32%). ^{1}H NMR (300 MHz, d^6-DMSO, 298 K, δ in ppm, numbering following Fig. 1): 13.41 (s, 1H, O*H*), 8.74 (s, 1H, C7–*H*), 8.55 (d, J_1 = 4.83 Hz, 1 H, C12–*H*), 7.80 (m, 1 H, C14–*H*), 7.50 (dd, J_1 = 7.60 Hz, J_2 = 1.59 Hz, 1 H, C3–*H*), 7.35 (m, 2 H, C15–*H*, C13–*H*, C6–*H*), 6.91 (m, 2 H, C4–*H*, C5–*H*), 4.91 (s, 2 H, C9–*H*). ^{13}C NMR (300 MHz, d^6-DMSO, 298 K, in ppm): 167.42 (*C*7), 160.52 (*C*2), 157.78 (*C*10), 149.26 (*C*12), 136.99 (*C*14), 132.50 (*C*13), 131.79 (*C*3), 122.49 (*C*6), 122.09 (*C*15), 118.72 (*C*1), 118.64 (*C*4), 116.47 (*C*5), 63.86 (*C*9). $C_{13}H_{12}N_2O$ (212.25) calcd: C 73.57, N 13.20, H 5.70; found C 72.97, N 11.44, H 5.45. FTIR (KBr, cm^{-1}): 3057 (m, br, OH), 2867 (m) 1630 (s, C=N), 1589 (m), 1491 (m), 1474 (m), 1458 (m), 1435 (m), 1389 (w), 1335 (w), 1279 (m), 1259 (w), 1220 (w), 1151 (w), 1116 (w), 1099 (w), 1047 (m), 1007 (w), 893 (w), 839 (w), 802 (m), 754 (s). Yellow single crystals (plates) were obtained by recrystallization in hot hexane after slow evaporation.

N-Salicylidene 3-aminomethylpyridine (**CH$_2$L^3**): 3-Aminomethylpyridine (2.40 mL, 1 equiv., 23.56 mmol) was dissolved in benzene (100 mL) in a 250 mL round-bottom flask with a Dean–Stark setup. Salicylaldehyde (2.48 mL, 1 equiv., 23.56 mmol) was added to the solution giving rise to an immediate coloration change to yellow. After refluxing the mixture for 24 h, the dark yellow solution was evaporated to give a crude solid which was triturated in hexane affording pure **CH$_2$L^3** as a strongly yellow microcrystalline powder (4.99 g, 99%). ^{1}H NMR (300 MHz, d^6-DMSO, 298 K, δ in ppm, numbering following cif files available in ref. 20): 13.22 (s, 1 H, O*H*), 8.76 (s, 1 H, C7–*H*), 8.60 (d, J_1 = 1.90 Hz, 1 H, C11–*H*), 8.51 (dd, J_1 = 4.8 Hz, J_2 = 1.6 Hz, 1 H, C10–*H*), 7.76 (d, J_1 = 7.9 Hz, 1 H, C12–*H*), 7.49 (dd, J_1 = 7.65 Hz, J_2 = 1.68 Hz, 1 H, C12–*H*), 7.42 (dd, 1 H, J_1 = 6.36 Hz, J_2 = 0.48 Hz, C5–*H*), 7.35 (m, 2H, C3–*H* and C13–*H*), 6.92 (m, 2H, C2–*H* and C4–*H*), 4.85 (s, 2 H, C8–*H*). ^{13}C NMR (300 MHz, d^6-DMSO, 298 K, δ in ppm): 168.36 (*C*7), 161.56 (*C*4), 150.34 (*C*11), 149.78 (*C*10), 136.84 (*C*12), 135.52 (*C*1), 133.79 (*C*3), 133.06 (*C*5), 124.97 (*C*13), 120.01 (*C*9), 119.93 (*C*6), 117.68 (*C*2), 60.67 (*C*8). $C_{13}H_{12}N_2O$ (212.25) calcd: C 73.57, N 13.20, H, 5.70; found: C 73.12, N 12.87, H 5.59. X-ray powder diffraction (°): 9.66 (m), 15.18 (w), 17.92 (m), 19.34 (m), 19.70 (m), 20.50 (m), 21.18 (w), 21.62 (m), 23.86 (s), 27.42 (m), 32.98 (m). FTIR (KBr, cm^{-1}): 3030 (w, br, OH), 2891 (w), 1630 (s, C=N), 1575 (m), 1491 (m), 1458 (m), 1421 (m), 1400 (m), 1350 (w), 1317 (w), 1275 (m), 1213 (w), 1198 (w), 1147 (w), 1113 (w), 1057 (m, C–O), 1028 (m), 993 (m), 970 (w), 924 (w), 876 (m), 856 (m), 795 (m), 770 (s), 712 (m). Yellow single crystals (plates) were obtained by recrystallization in hot hexane after slow evaporation. An X-ray investigation has revealed the same cell parameters as those in ref. 31.

N-Salicylidene 4-aminomethylpyridine (**CH$_2$L^4**): 4-Aminomethylpyridine (2.38 mL, 1 equiv., 23.56 mmol) was dissolved in benzene (100 mL) in a 250 mL round bottom flask with a Dean–Stark setup. Salicylaldehyde (2.48 mL, 1 equiv., 23.56 mmol) was added in the mixture which immediately turned to yellow. After refluxing for 24 h, the solution was concentrated leading to a yellow solid which was triturated in hexane in order to obtain pure **CH$_2$L^4** as a pale yellow powder (4.90 g, 98%). ^{1}H NMR (300 MHz, d^6-DMSO, 298 K, δ in ppm): 13.20 (s, 1H, O*H*), 8.73 (s, 1 H, N=C*H*), 8.56 (dd, J_1 = 4.41 Hz, J_2 = 1.62 Hz, 2 H, N–CH$_2$–C–CH–C*H*), 7.49 (m, 1 H, N=CH–C–C*H*), 7.35 (m, 3 H, HO–C–CH–C*H* and N–CH$_2$–C–CH–C*H*), 6.93 (m, 2 H, HO–C–C*H* and HO–C–CH–CH–C*H*), 4.91 (s, 2 H, N–C*H*$_2$). ^{13}C NMR (300 MHz, d^6-DMSO, 298 K, δ in ppm): 167.75 (N=*C*H), 160.31 (HO–*C*), 149.83 (N–CH$_2$–C–CH–*C*H), 147.59 (HO–C–*C*), 132.66 (N–CH$_2$–C–*C*H), 131.86 (N=CH–C–*C*H), 122.67 (HO–C–CH–*C*H), 118.84 (HO–C–CH–CH–*C*H), 118.69 (N–CH$_2$–*C*), 116.47 (HO–C–*C*H), 60.68 (N–*C*H$_2$). MS: m/z = 213 (M + H$^+$), 196 ($C_{13}H_{10}N_2$). Purity checked in HRMS (TOF MS ES+): m/z = 213.1025 (calculated: 213.1028). FTIR (KBr, cm^{-1}): 3049 (m, br, OH), 2868 (m), 2725 (m, br), 1630 (s), 1602 (s, C=N), 1580 (m), 1489 (m), 1458 (s), 1413 (m), 1389 (w), 1279 (m), 1250 (m), 1219 (w), 1151 (w, C–O), 1116 (w), 1065 (w), 1034 (m), 1009 (w), 800 (m), 754 (s).

5-Chloro-*N*-salicylidene 3-aminomethylpyridine (**CH$_2$L^{3}Cl**): 3-Aminomethylpyridine (2.40 mL, 1 equiv., 23.56 mmol) was dissolved in benzene (70 mL) in a 250 mL round bottom flask with a Dean–Stark setup. 5-Chloro-salicylaldehyde (3.69 g, 1 equiv., 23.56 mmol) was added to the mixture which immediately turned to dark yellow. After refluxing for 24 h, the solution was concentrated leading to a dark crude oil which was triturated in hexane in order to obtain pure **CH$_2$L^{3}Cl** as a yellow microcrystalline powder (5.44 g, 93%). ^{1}H NMR (300 MHz, d^6-DMSO, 298 K, δ in ppm, numbering following Fig. 2): 8.76 (s, 1 H, C8–*H*), 8.59 (d, J_1 = 1.80 Hz, 1 H, C13–*H*), 8.51 (dd, J_1 = 4.80 Hz, J_2 = 1.60 Hz, 1 H, C11–*H*), 7.76 (dt, J_1 = 7.83 Hz, J_2 = 1.83 Hz, 1 H, C14–*H*), 7.61 (d, J_1 = 2.67 Hz, 1 H, C6–*H*), 7.40 (m, 2 H, C15–*H*, C4–*H*), 6.92 (d, J_1 = 8.85 Hz, 1 H, C3–*H*), 4.85 (s, 2 H, C9–*H*). ^{13}C NMR (300 MHz, d^6-DMSO, 298 K, δ in ppm): 165.67 (*C*7), 159.12 (*C*5), 149.13 (*C*13), 148.59 (*C*11), 135.66 (*C*14), 134.04 (*C*2), 132.15 (*C*4), 130.56 (*C*6), 123.72 (*C*15), 121.01 (*C*1), 119.84 (*C*10), 118.48 (*C*3), 61.58 (*C*9). $C_{13}H_{12}N_2O$ (212.25) calcd: C 63.29, N 11.36, H 4.43; found: C 63.29, N 11.49, H 4.43. X-ray powder diffraction (°): 6.6 (s), 13.12 (w), 16.14 (m), 16.84 (w), 19.62 (m), 20.5 (m), 20.84 (w), 21.62 (s), 24.00 (s), 24.10 (m), 25.02 (m), 25.46 (m), 25.74 (m), 26.12 (s), 28.16 (m), 29.16 (m), 30.08 (m), 30.16 (m), 30.54 (w), 32.26 (m), 35.64 (w), 36.46 (w), 39.56 (w), 41.84 (w), 44.34 (w), 45.04 (w), 48.20 (w), 49.48 (w). FTIR (KBr, cm^{-1}): 3057 (w, br, OH), 2995 (w), 2914 (w), 2850 (w), 1633 (s, C=N), 1576 (m), 1558 (w), 1448 (w), 1450 (m), 1416 (m), 1394 (w), 1369 (m), 1338 (m), 1308 (w), 1277 (s), 1232 (w), 1203 (w), 1184 (m), 1107 (m), 1092 (w), 1036 (m), 1022 (s), 955 (w), 910 (w), 891 (w), 833 (w), 820 (s), 802 (m), 777 (w), 716 (m), 710 (s). Yellow single crystals (long needles) were obtained by recrystallization in hot hexane after slow solvent evaporation.

5-Chloro-*N*-salicylidene 4-aminomethylpyridine (**CH$_2$L^{4}Cl**): 4-Aminomethylpyridine (2.38 mL, 1 equiv., 23.56 mmol) was dissolved in benzene (70 mL) in a 250 mL round bottom flask with a Dean–Stark setup. 5-Chloro-salicylaldehyde (3.69 g, 1 equiv., 23.56 mmol) was added to the mixture which immediately turned to yellow. After refluxing for 24 h, the solution was concentrated giving crude orange oil which was triturated in hexane affording pure **CH$_2$L^{4}Cl** as a yellow microcrystalline powder (5.48 g, 94%). ^{1}H NMR (300 MHz, d^6-DMSO, 298 K, δ in ppm): 13.11 (s, 1 H, O*H*), 8.73 (s, 1 H, N=C*H*), 8.56 (m, 2 H, N–CH$_2$–C–CH–C*H*), 7.63 (d, J_1 = 3 Hz, 1 H, N=CH–C–C*H*), 7.36 (m, 3 H, N–CH$_2$–C–C*H* and HO–C–CH–C*H*), 6.95 (d, J_1 = 8.85 Hz, 1 H, HO–C–C*H*), 4.85 (s, 2 H, N–C*H*$_2$). ^{13}C NMR (300 MHz, d^6-DMSO, 298 K, δ in ppm): 167.22 (N=*C*H), 160.05 (HO–*C*), 150.79 (N–CH$_2$–C–CH–*C*H),

147.30 (HO–C–*C*), 133.21 (N–CH_2–C–*C*H), 131.50 (N=CH–C–*C*H), 123.64 (HO–C–CH–*C*H), 121.79 (Cl–*C*), 120.86 (N–CH_2–*C*), 119.49 (HO–C–*C*H), 61.58 (N–*C*H_2). MS: *m*/*z* = 247 ($M - H^+$), 230 ($C_{13}H_9N_2Cl$), 210 ($C_{13}H_{10}N_2O$). $C_{13}H_{12}N_2O$ (212.25) calcd: C 63.29, N 11.36, H 4.43; found: C 63.81, N 12.15, H 4.70. X-ray powder diffraction (°): 6.74 (w), 16.06 (m), 16.78 (w), 19.60 (m), 20.60 (w), 21.60 (w), 21.64 (s), 23.98 (m), 25.10 (m), 25.22 (m), 26.16 (m), 26.22 (m), 28.18 (w), 29.14 (m), 30.08 (m), 30.16 (m), 30.24 (w), 32.36 (m), 35.64 (w), 39.62 (w), 41.96 (w), 44.34 (w), 44.44 (m), 46.74 (w), 49.48 (w). FTIR (KBr, cm^{-1}): 3069 (w, br, OH), 2922 (w), 2899 (w), 2856 (w), 1633 (s, C=N), 1597 (m), 1575 (w), 1560 (m), 1481 (s), 1450 (m), 1416 (m), 1389 (m), 1367 (m), 1337 (m), 1327 (w), 1308 (w), 1277 (s), 1219 (m), 1182 (m), 1117 (w), 1092 (m), 1068 (w), 1032 (m), 991 (m), 960 (m), 889 (w), 827 (m), 808 (m), 777 (w), 706 (m).

X-Ray crystallography

X-ray intensity data were collected at 125 K for $\mathbf{CH_2L^2}$ and 120 K for $\mathbf{CH_3L^3Cl}$ with a MAR345 image plate using Mo-Kα (λ = 0.71069 Å) radiation. The crystal was chosen, mounted in inert oil and transferred to the cold gas stream for flash cooling. The crystal data and the data collection parameters are summarized in Table 1. The unit cell parameters were refined using all collected spots after the integration process. The structures were solved by direct methods and refined by full-matrix least-squares on F^2 using SHELXL97.[48] All non-hydrogen atoms were refined anisotropically. Hydrogen atoms were localized by Fourier difference and included in the refinement with a common isotropic temperature factor. The details of the refinements and the final *R* indices are presented in Table 1.

Acknowledgements

This work was partly funded by the Fonds de la Recherche Scientifique-FNRS (FRFC No 2.4508.08, No 2.4537.12, IISN 4.4507.10) and ARC-Louvain. We also thank the Fonds pour la Formation à la Recherche dans l'Industrie et dans l'Agriculture for doctoral scholarships allocated to F.R and P.-L. J.

References

1 (*a*) G. H. Brown, *Photochromism*, Wiley, New York, 1971; (*b*) H. Dürr, B. Laurent, *Photochromism: Molecules and Systems*, Elsevier, Amsterdam, The Netherlands, 2nd edn, 2003.
2 O. Sato, *J. Photochem. Photobiol., C*, 2004, **5**, 203.
3 T. He and J.-N. Yao, *J. Mater. Chem.*, 2007, **17**, 4547.
4 P. Gütlich, Y. Garcia and T. Woike, *Coord. Chem. Rev.*, 2001, **219–221**, 839.
5 M. Irie, *Chem. Rev.*, 2000, **100**, 1683.
6 O. Sato, *Acc. Chem. Res.*, 2003, **36**, 692.
7 R. Klajn, P. J. Wesson, K. J. M. Bishop and B. A. Grzybowski, *Angew. Chem., Int. Ed.*, 2009, **48**, 7035.
8 S. Venkatarami, U. Jana, M. Dommascheck, D. F. Schönnischen, F. Tuczek and R. Herges, *Science*, 2011, **331**, 445.
9 K. Amimoto and T. Kawato, *J. Photochem. Photobiol. C*, 2005, **6**, 207.
10 (*a*) K. Matsuda and M. Irie, *Chem. Lett.*, 2000, **16;** (*b*) K. Matsuda and M. Irie, *J. Am. Chem. Soc.*, 2000, **122**, 7195; (*c*) K. Matsuda and M. Irie, *Mol. Cryst. Liq. Cryst.*, 2000, **345**, 155; (*d*) K. Matsuda and M. Irie, *Polyhedron*, 2001, **20**, 1391; (*e*) K. Matsuda and M. Irie, *Chem.–Eur. J.*, 2001, **7**, 3466; (*f*) K. Takayama, K. Matsuda and M. Irie, *Chem.–Eur. J.*, 2003, **9**, 5605.
11 Y. Garcia, V. Ksenofontov, R. Lapouyade, A. D. Naik, F. Robert and P. Gütlich, *Opt. Mater.*, 2011, **33**, 942.
12 B. L. Feringa, W. F. Jager and B. de Lange, *Tetrahedron*, 1993, **49**, 8267.
13 S. Kawata and Y. Kawata, *Chem. Rev.*, 2000, **100**, 1777.
14 B. L. Feringa, *Acc. Chem. Res.*, 2001, **34**, 504.
15 (*a*) M. Irie, in *Molecular Switches*, ed. B. L. Feringa, Wiley-VCH, Weinheim, 2001, p. 37; (*b*) K. Matsuda and M. Irie, in *Chemistry of Nano-molecular System - Towards the Realization of Molecular Devices*, ed. T. Nakamura, T. Matsumoto, H. Tada and K.-I. Sugiura, Springer, 2002, p. 25.
16 (*a*) J. Yao, K. Hashimoto and A. Fujishima, *Nature*, 1992, **355**, 624; (*b*) C. Bechinger, S. Ferrer, A. Zaban, J. Sprague and B. A. Gregg, *Nature*, 1996, **383**, 608.
17 V. A. Bren, A. D. Dubonosov, V. I. Minkin, T. N. Gribanova, V. P. Rybalkin, E. N. Shepelenko, A. V. Tsukanov and R. N. Borisenko, *Mol. Cryst. Liq. Cryst.*, 2005, **431**, 417.
18 (*a*) K. Nakatani and J. A. Delaire, *Chem. Mater.*, 1997, **9**, 2682; (*b*) J. A. Delaire and K. Nakatani, *Chem. Rev.*, 2000, **100**, 1817.
19 (*a*) M. D. Cohen and G. M. J. Schmidt, *J. Phys. Chem.*, 1962, **66**, 2442; (*b*) M. D. Cohen, G. M. J. Schmidt and S. Flavian, *J. Chem. Soc.*, 1964, 2041; (*c*) M. D. Cohen, Y. Hirshberg and G. M. J. Schmidt, *J. Chem. Soc.*, 1964, 2051; (*d*) M. D. Cohen, Y. Hirshberg and G. M. J. Schmidt, *J. Chem. Soc.*, 1964, 2060; (*e*) J. Bregman, L. Leiserowitz and G. M. J. Schmidt, *J. Chem. Soc.*, 1964, 2068; (*f*) M. D. Cohen and S. Flavian, *J. Chem. Soc. B*, 1967, 317; (*g*) M. D. Cohen and S. Flavian, *J. Chem. Soc. B*, 1967, 321; (*h*) M. D. Cohen, S. Flavian and L. Leiserowitz, *J. Chem. Soc. B*, 1967, 329; (*i*) M. D. Cohen and S. Flavian, *J. Chem. Soc. B*, 1967, 334; (*j*) M. D. Cohen, *J. Chem. Soc. B*, 1968, 373.
20 *Organic Photochromic and Thermochromic Compounds*, ed. J. C. Cran, and R. J. Guglielmetti, vol. **2**, Plenum Press, New York, 1999.
21 M. Mikami and S. Nakamura, *J. Phys. Chem. B*, 2004, **33**, 579.
22 E. Hadjoudis, *Mol. Eng.*, 1995, **5**, 301.
23 T. Fujiwara, J. Hadara and O. Keiichiro, *J. Phys. Chem. B*, 2004, **108**, 4035.
24 M. E. Kletskii, A. A. Millov, A. V. Metelitsa and M. I. Knyazhansky, *J. Photochem. Photobiol., A*, 1997, **110**, 267.
25 N. Otsubo, C. Okabe, H. Mori, K. Sakota, K. Amimoto, T. Kawato and H. Sekiya, *J. Photochem. Photobiol., A*, 2002, **154**, 33.
26 V. C. Vargas, *J. Phys. Chem. A*, 2004, **108**, 281.
27 E. Hadjoudis, M. Vittorakis and I. Moustakali-Mavridis, *Tetrahedron*, 1987, **43**, 1345.
28 F. Robert, A. D. Naik, F. Hidara, B. Tinant, R. Robiette, J. Wouters and Y. Garcia, *Eur. J. Org. Chem.*, 2010, 621.
29 (*a*) E. Hadjoudis and I. M. Mavridis, *Chem. Soc. Rev.*, 2004, **33**, 579; (*b*) E. Hadjoudis, S. D. Chatziefthimiou and I. M. Mavridis, *Curr. Org. Chem.*, 2009, **13**, 269.
30 F. Robert, A. D. Naik, B. Tinant, R. Robiette and Y. Garcia, *Chem.–Eur. J.*, 2009, **15**, 4327.
31 Z. Cimerman, R. Kiralj and N. Galic, *J. Mol. Struct.*, 1994, **323**, 7.
32 E. Lambi, D. Gegiou and E. Hadjoudis, *J. Photochem. Photobiol., A*, 1995, **86**, 241.
33 R. W. Oehmke and J. C. Baillard, *J. Inorg. Nucl. Chem.*, 1965, **27**, 2209.
34 L. Shi, H. M. Ge, S. H. Tan, H. Q. Li, Y. C. Song, H. L. Zhu and R. X. Tan, *Eur. J. Med. Chem.*, 2007, **42**, 558.
35 E. Hadjoudis, V. Verganelakis, C. Trapalis and G. Kordas, *Mol. Eng.*, 1999, **8**, 459.
36 L. Z. Zhang, Y. Xiang, P. Cheng, G. Q. Tang and D. Z. Liao, *Chem. Phys. Lett.*, 2002, **358**, 278.
37 S. Sakagami, T. Koga and A. Takase, *Mol. Cryst. Liq. Cryst.*, 2002, **373**, 71.
38 M. Ziółek and I. Sobczak, *J. Inclusion Phenom. Macrocyclic Chem.*, 2009, **63**, 211.
39 F. Robert, A. D. Naik, B. Tinant and Y. Garcia, *Inorg. Chim. Acta*, 2012, **380**, 104.
40 E. Lambi, D. Gegiou and E. Hadjoudis, *J. Photochem. Photobiol., A*, 1995, **86**, 241.
41 J. Harada, T. Fujiwara and K. Ogawa, *J. Am. Chem. Soc.*, 2007, **129**, 16216.
42 T. Sekikawa, T. Kobayashi and T. Inabe, *J. Phys. Chem. A*, 1997, **101**, 644.
43 M. E. Kletskii, A. A. Millov, A. V. Metelitsa and M. I. Knyazhansky, *J. Photochem. Photobiol., A*, 1997, **110**, 267.

44 (*a*) T. Haneda, M. Kawano, T. Kojima and M. Fujita, *Angew. Chem., Int. Ed.*, 2007, **46**, 6643; (*b*) Y. Inokuma, M. Kawano and M. Fujita, *Nat. Chem.*, 2011, **3**, 349.
45 F. Robert, B. Tinant, R. Clérac, P.-L. Jacquemin and Y. Garcia, *Polyhedron*, 2010, **29**, 2739.
46 F. Robert, A. D. Naik and Y. Garcia, *J. Phys.: Conf. Ser.*, 2010, **217**, 012031.
47 Y. Garcia, F. Robert, A. D. Naik, G. Zhou, B. Tinant, K. Robeyns, S. Michotte and L. Piraux, *J. Am. Chem. Soc.*, 2011, **133**, 15850.
48 G. M. Sheldrick, *SHELXS-97, Program for solution of crystal structures*, University of Göttingen, Germany, 1997; G. M. Sheldrick, *SHELXL-97, Program for refinement of crystal structures*, University of Göttingen, Germany, 1997.